http://dx.doi.org/10.5012/bkcs.2012.33.12.4084

Substituent Effect on the Structure and Biological Property of ^{99m}Tc-Labeled Diphosphonates: Theoretical Studies

Ling Qiu,[*] Jian-Guo Lin,[*] Xue-Dong Gong,[†] Wen Cheng, and Shi-Neng Luo

Key Laboratory of Nuclear Medicine, Ministry of Health, Jiangsu Key Laboratory of Molecular Nuclear Medicine, Jiangsu Institute of Nuclear Medicine, Wuxi 214063, P.R. China
[*]E-mail: qiulingwx@gmail.com (L. Q), jglin@yahoo.cn (J.G. L)
[†]Institute for Computation in Molecular and Material Science, School of Chemical Engineering, Nanjing University of Science and Technology, Nanjing 210094, P.R. China
Received May 24, 2012, Accepted September 21, 2012

Theoretical calculations based on density functional theory (DFT) were performed to study the substituent effect on the geometric and electronic structures as well as the biological behavior of technetium-99m-labeled diphosphonate complexes. Optimized structures of these complexes are surrounded by six ligands in an octahedral environment with three unpaired 4d electrons (d^3 state) and the optimized geometry of ^{99m}Tc-MDP agrees with experimental data. With the increase of electron-donating substituent or tether between phosphate groups, the energy gap between frontier orbitals increases and the probability of non-radiative deactivation *via* d-d electron transfer decreases. The charge distribution reflects a significant ligand-to-metal electron donation. Based on the calculated geometric and electronic structures and biologic properties of ^{99m}Tc-diphosphonate complexes, several structure-activity relationships (SARs) were established. These results may be instructive for the design and synthesis of novel ^{99m}Tc-diphosphonate bone imaging agent and other ^{99m}Tc-based radiopharmaceuticals.

Key Words : Bone imaging agent, ^{99m}Tc-diphosphonate, Substituent effect, SAR, DFT

Introduction

In the past few years, technetium-99m-based radiopharmaceuticals have received considerable attention as diagnostic agents in nuclear medicine due to the favorable nuclear properties (E_γ = 142 keV, $t_{1/2}$ = 6.02 h) and low cost of the radionuclide ^{99m}Tc.[1-3] A variety of ^{99m}Tc-based radiopharmaceuticals have been developed and approved by the Federal Drug Administration (FDA) for determining organ function or assessing disease status by imaging methods.[4-6] Bone imaging agents are among the first developed ^{99m}Tc-radiopharmaceuticals and the most widely used radiopharmaceuticals in the diagnostic nuclear medicine,[4] which involve ^{99m}Tc-labeled diphosphonates such as methylenediphosphonate (MDP)[7] and hydroxymethylenediphosphonate (HMDP).[8] They have been widely used for many years in bone scanning and provide an effective means of diagnosing primary bone cancer, metastatic bone disease, Paget's disease, osteoporosis, bone trauma, *etc.*

As well known, a successful bone imaging agent requires high bone uptake and low soft-tissue uptake as well as a quick clearance from the blood and soft tissues. However, in order to achieve images of high definition, current agents normally require an interval of 2-6 h between injecting and performing the bone scanning.[9] Therefore, shortening this interval is highly desirable that could lead to worthwhile increases in convenience to patients and physicians and in the efficiency of running nuclear medicine units. Accordingly, a radiopharmaceutical with higher affinity for bone, larger uptake ratios of bone-to-soft tissues and more rapid clearance from blood is required to enable imaging at an earlier time post injection.[10] To date, a number of ^{99m}Tc-labeled diphosphonates have been prepared and evaluated in animals.[5,9-11] We have also been involved for several years in the synthesis and biological evaluation of novel ^{99m}Tc-diphosphonate complexes for developing novel bone imaging agents.[11] In general, all of these compounds have the phosphate groups separated by a single carbon atom, *i.e.*, with the fundamental P-C-P backbone structure. What about increasing the number of tether between two phosphates? So far, there are few studies reported.[12,13]

As an adjunct to experiment for the design and analysis of novel compounds, molecular modeling has found extensive use in the organic pharmaceuticals and other valuable chemicals.[14] This not only provides useful information that is difficult or impossible to measure, but also leads to a reduction in unnecessary measurement or synthesis of candidates in the course of designing new compounds. With the rapid development on the computer technology and theoretical chemistry, molecular modeling has also been used successfully in the metal-based diagnostic or therapeutic agents,[15,16] although there are several difficulties inherent in the transition metal chemistry, such as large number of electrons and orbitals, relativistic and electron correlation effects, and diverse open-shell species. As expected by Jurisson in the review of coordination compounds in nuclear medicine, "molecular modeling will certainly become an important aspect of the design process".[17]

Table 1. Schematic illustration of molecular structures of ^{99m}Tc-DPs

Compd.	Code	Name	Description
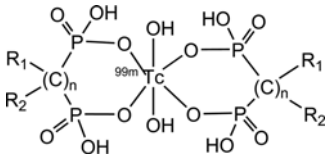	^{99m}Tc-MDP	^{99m}Tc-methylene-1,1-diphosphonic acid	n=1, R_1=R_2=H
	^{99m}Tc-HMDP	^{99m}Tc-hydroxymethylene-1,1-diphosphonic acid	n=1, R_1=OH, R_2=H
	^{99m}Tc-HEDP	^{99m}Tc-hydroxyethane-1,1-diphosphonic acid	n=1, R_1=OH, R_2=CH_3
	^{99m}Tc-DHPE	^{99m}Tc-1,2-dihydroxy-1,2-bis(dihydroxyphosphonyl)ethane	n=2, $^{1,2}R_1$=OH, $^{1,2}R_2$=H
	^{99m}Tc-DHPB	^{99m}Tc-2,3-dihydroxy-2,3-bis(dihydroxyphosphonyl)butane	n=2, $^{2,3}R_1$=OH, $^{2,3}R_2$=CH_3
	^{99m}Tc-DHPP	^{99m}Tc-2,4-dihydroxy-2,4-bis(dihydroxyphosphonyl)pentane	n=3, $^{2,4}R_1$=OH, $^{2,4}R_2$=CH_3; $^{3}R_1$=$^{3}R_2$=H

In a continuing effort to find better bone-imaging agents, in the present work molecular modeling was performed to investigate the effect of tether between two phosphates on the geometric and electronic structures as well as the biological behavior of ^{99m}Tc-labled diphosphonate complexes, such as ^{99m}Tc-labeled 1,2-dihydroxy-1,2-bis(dihydroxyphosphonyl)ethane (DHPE),[12] 2,3-dihydroxy-2,3-bis(dihydroxyphosphonyl) butane (DHPB),[13] and 2,4-dihydroxy-2,4-bis-(dihydroxyphosphonyl)pentane (DHPP).[13] These compounds can be viewed as longer-chain analogues of MDP with the backbone P-C_n-P (see Table 1). Besides, ^{99m}Tc-HMDP[8] and ^{99m}Tc-HEDP[18] with the methylene-hydrogen atoms substituted by -OH and -CH_3 have also been studied. Substituent effect on the structures and biological behavior was investigated and compared with available experimental data. The structure-activity relationship has also been established for these complexes, which may be instructive for the design and synthesis of novel ^{99m}Tc-diphosphonate bone imaging agent and other ^{99m}Tc-based radiopharmaceuticals.

Computational Methods

According to the X-ray structure of the clinically widely-used bone imaging agent ^{99m}Tc-MDP,[19] structures of ^{99m}Tc-MDP, ^{99m}Tc-HMDP, ^{99m}Tc-HEDP, ^{99m}Tc-DHPE, ^{99m}Tc-DHPB and ^{99m}Tc-DHPP were constructed using the 3D Build tools as implemented in the Visualizer module of the commercial software Materials Studio 3.0.1.[20] The initial models were optimized by molecular mechanics (MM) method with the Universal forcefield[21] using the Forcite module. Then, every conformer was reoptimized by the hybrid B3LYP[22] method with the Gaussian03 program.[23] To include the technetium-containing model system in the quantum chemical (QM) calculation, the "double-ξ" quality basis set LANL2DZ[24] was chosen which uses Dunning D95V basis set[25] on first row atoms and Los Alamos effective core potential (ECP) plus DZ on Na-Bi.[26] Compared to all-electron basis sets, ECPs account to some extent for relativistic effects, which are believed to become important for the elements from the fourth row of the periodic table. Geometries were fully optimized without any symmetry restriction by the Berny method, and the nature of the stationary point was verified through the harmonic vibration analysis. Charge distribution in each complex was studied by Mulliken population analysis (MPA)[27] as implemented in the Gaussian03 program package.[23] The electron density diagrams of molecular orbitals were generated by the GaussView program.[28] Based on the B3LYP/LANL2DZ optimized structures, several physicochemical parameters were further computed by the QSAR properties item of Hyperchem7.5[29] to study the structure-activity relationship of ^{99m}Tc-DPs.

Results and Discussion

Ground-State Geometry. As well known, the first and most important step in any computer-aided design and analysis protocol is to determine reasonable geometries of the target compounds. With respect to ^{99m}Tc-DPs in the present study, *syn* and *anti* isomers may be existed for each complex except ^{99m}Tc-MDP that is defined by the relative spatial orientation of the hydroxyl group (*i.e.*, R_1) on the carbon atom to that of the hydroxyl on the center metal Tc. In Figure 1S, the fully optimized ground-state geometries are shown for the *syn* and *anti* isomers. There are no imaginary frequencies for any structure, indicating that these structures are indeed the minima on their potential energy surfaces. The main optimized geometric parameters in the gas phase together with the X-ray crystal diffraction data of the complex $[Li(H_2O)_3][^{99}Tc^{IV}(OH)(MDP)]\cdot{}^{1}/_{3}H_2O$[19] are listed in Table 2.

In each optimized complex, Tc(IV) adopts an octahedral coordination geometry with one technetium center bridging two DPs and two hydroxyl groups. The basal plane is defined by four oxygen atoms (O4, O6, O12 and O18) of the DP and hydroxyl ligands, and the apical positions are occupied by another two oxygen atoms (O14 and O19) of the DP and hydroxyl ligands. Inspecting the optimized structure of the prototypical complex ^{99m}Tc-MDP, the calculated Tc-O bond lengths are found to vary from 2.007 to 2.088 Å, which are generally in line with the observed Tc-O single bond lengths (2.00-2.03 Å)[30] since Tc=O double bond lengths are considerably shorter (1.65-1.70 Å).[30] Compared with the experi-

Table 2. Optimized geometric parameters (length in Å and angle in degree) of Tc-DPs

	^{99m}Tc-MDP		^{99m}Tc-HMDP		^{99m}Tc-HEDP		^{99m}Tc-DHPE		^{99m}Tc-DHPB		^{99m}Tc-DHPP	
	Cal.	Exp.	*syn*	*anti*	*syn*	*anti*	*syn*	*anti*	*syn*	*anti*	*syn*	*anti*
Bond Length												
Tc-O(4)	2.007	2.000(14)	2.020	2.042	2.023	2.043	2.044	2.011	2.011	2.021	2.019	2.033
Tc-O(6)	2.019	2.036(16)	2.044	2.015	2.041	2.029	1.991	2.057	1.997	2.071	2.005	2.034
Tc-O(12)	2.019	2.029(12)	2.045	2.042	2.058	2.038	2.013	2.072	1.998	2.043	1.999	1.991
Tc-O(14)	2.007	1.983(14)	2.014	2.026	1.995	2.030	2.029	1.982	2.035	1.991	1.999	1.983
Tc-O(18)	2.088	1.968(15)	2.045	2.023	2.043	2.023	2.086	2.005	2.072	2.043	2.097	2.095
Tc-O(19)	2.088	1.917(12)	2.029	2.037	2.043	2.030	2.041	2.025	2.064	2.018	2.074	2.019
A[a]	2.013	2.066(14)	2.031	2.031	2.029	2.035	2.019	2.031	2.010	2.032	2.006	2.010
B[b]	2.088	1.943(14)	2.037	2.030	2.043	2.027	2.064	2.015	2.068	2.031	2.086	2.057
Bond Angle												
O(4)-Tc-O(6)	90.33		91.98	90.32	92.34	87.78	92.45	87.91	89.47	85.13	93.08	92.09
O(4)-Tc-O(12)	96.76		95.48	93.82	93.33	96.73	96.53	88.96	96.25	87.17	89.99	89.18
O(4)-Tc-O(14)	92.75		93.46	90.58	90.16	92.96	89.92	88.89	90.29	91.84	90.99	93.11
O(4)-Tc-O(18)	176.23		175.52	178.66	178.15	174.57	175.79	172.76	174.99	173.74	176.87	174.23
O(4)-Tc-O(19)	88.29		85.25	86.73	86.08	86.33	88.16	93.98	89.62	95.26	91.98	89.47
O(18)-Tc-O(19)	90.90		90.41	94.13	94.38	90.14	93.23	89.33	91.33	88.18	88.88	86.59

[a]A = mean value of Tc-O_{DP} bonds. [b]B = mean value of Tc-O_{OH} bonds.

mental values ranging from 1.917 to 2.036 Å,[19] the optimized Tc-O bond distances are slightly longer. This is not surprising given that crystal packing and hydrogen bonds can induce conformational features that are not present in the theoretical calculation of the isolated molecule in the gas phase at 0 K. Additionally, there is also inherent drawback in the DFT calculations arising from the dynamical correlation effects.[31] On the other hand, the calculated bond lengths and bond angles within the MDP ligand are in general agreement with the experimental studies of the free acid H_4MDP[32] and related diphosphonates.[33] A slight discrepancy comes from the crystal lattice distortion existing in the real molecules. On the whole, the fully optimized complex Tc-MDP is in general agreement with the experimental structure. Therefore, it was used as a starting point to investigate the relative stability of Tc(IV) complexes with different diphosphonate ligands and to evaluate the stabilizing or destabilizing influence of various functional groups combined to the carbon atom of MDP.

From Tc-MDP to Tc-HMDP and to Tc-HEDP with the methylene-hydrogen atoms substituted by -OH and -CH_3, the atomic distances between Tc and O_{DP} increase while those between Tc and O_{OH} decrease (see Table 2). This indicates that the bond strength of Tc-O_{DP} in Tc-HMDP and Tc-HEDP becomes weaker in comparison with the parent complex Tc-MDP, while Tc-O_{OH} in Tc-HMDP and Tc-HEDP are stronger than that of Tc-MDP. This may be due to the increase of steric hindrance caused by the additional substituent at the carbon atom. Comparison between *syn* and *anti* isomers shows that the bond lengths of Tc-O_{DP} arrange differently due to the different orientation of side chains in the *syn* and *anti* isomers. For example, in the *syn* and *anti* isomers of Tc-HMDP, although the individual bond lengths of Tc-O_{DP} display significant differences, the mean values are equal. Also noteworthy is that some Tc-O_{DP} bonds in the *anti* isomer of Tc-HEDP are even longer than those in the *syn* isomer. This may be attributed to the larger steric hindrance of the methyl than the hydroxyl. Moreover, the bond lengths of Tc-O_{OH} in the *anti* isomer are shorter than those in the *syn* one. According to the definition of *syn* and *anti* isomers, it can be interpreted by the fact that the *syn* isomer has more hydroxyl groups at the same side than the *anti* isomer, and therefore the repulsion between these groups in the *syn* isomer are larger than those in the *anti* isomer. This can be observed intuitively from the optimized geometries of Tc-HMDP and Tc-HEDP (Figure 1S).

As the tether between two phosphate groups increases from one to three, *i.e.*, from Tc-HMDP and Tc-HEDP to Tc-DHPE, Tc-DHPB, and Tc-DHPP, the bond lengths of Tc-O_{DP} are found to decrease and those of Tc-O_{OH} increase on the whole. On the one hand, this is mainly ascribed to the fact that the repulsion between atoms of the ligand and the center metal decreases with the expansion of the ring formed by Tc and DPs. On the other hand, it can also be explained in terms of electron density on the technetium, by considering the contribution of electron donation from the ligand with electron donating substituents (-OH, -CH_3 and -CH_2-) to the central technetium atom. An increase of the electron density on the technetium atom prevents σ and π electron donation from the hydroxyl group to the technetium atom, and it would lengthen the bond Tc-O_{OH} and shorten the bond Tc-O_{DP}. Similarly, comparison between *syn* and *anti* isomers also shows that Tc-O_{OH} bonds in the *anti* isomers are shorter than those in the *syn* one, and bond lengths of Tc-O_{DP} rearrange differently according to the different orientation of side chains in the *syn* and *anti* isomers. Due to the larger repulsion between atoms of the ligand and the center metal in the *anti* isomers (see Figure 1S), Tc-O_{DP} bonds in the *anti*

isomer of Tc-HEDP are even longer than those in the *syn* isomer.

Furthermore, there are fifteen bond angles about Tc in the ^{99m}Tc-labeled diphosphonate complex with the coordination mode MA_4B_2. Three of them have equilibrium values of 180º, and the rest have equilibrium values of 90º. According to calculations, the angles for these Tc-diphosphonate complexes showed a slight deviation from an ideal octahedral arrangement in accordance with the study of Alberto *et al.*[34] Table 2 also shows that although the methylene-hydrogen atoms are substituted by different groups or the tether between phosphate groups increases, they have similar geometrical rearrangements around the center metal to Tc-MDP and there is no significant difference in the bond angles O-Tc-O of the *syn* and *anti* isomers. Thus, they are independent of the electron-donating character and spatial orientation of the substituent in the DPs ligands.

Electronic Structure. Table 3 lists the energies of total electrons and frontier molecular orbitals (FMOs) as well as the energy gap between FMOs ($E_g = E_{LUMO} - E_{HOMO}$), where HOMO and LUMO denote the highest occupied molecular orbital and the lowest unoccupied molecular orbital. The charge distribution and spin density obtained from the Mulliken population analysis are given in Table 4.

Several features can be observed from Tables 3 and 4. First, total energies of all *anti* isomers are higher than those of the *syn* isomers, indicating the *anti* conformers of Tc-DPs are less stable than the *syn* ones. This is consistent with the fact that molecular polarities (μ) of the optimized *anti* structures are higher than those of the *syn* structures. However, the energy gaps E_g of *anti* isomers are all higher than those of *syn* isomers besides both E_{HOMO} and E_{LUMO} of the *anti* isomers are larger than those of the *syn* isomers, indicating that the *anti* isomer has higher stability than the *syn* isomer. Here, the stability refers to the chemical or photochemical processes with electron transfer or leap. That is, the probability of non-radiative deactivation *via* d-d electron transfer in the *syn* conformation is larger than that in the *anti* conformation. As well known, frontier molecular orbitals usually play a relevant role in such systems because they rule the electronic excitations and the transition character. To intuitively understand the electron transition process, Figure 1

Table 3. Energetic properties of Tc-DPs calculated at the B3LYP/LANL2DZ level

Conformer		E_T/a.u.	E_{HOMO}/a.u.	E_{LUMO}/a.u.	E_g/eV	μ/Debye
Tc-MDP		-1241.6367585	-0.0426	0.0846	3.4613	4.5634
Tc-HMDP	*syn*	-1392.0230285	-0.0479	0.0811	3.5084	4.7337
	anti	-1392.0113244	-0.0398	0.0899	3.5280	5.8944
Tc-HEDP	*syn*	-1470.6555748	-0.0445	0.0815	3.4303	4.6092
	anti	-1470.6333773	-0.0342	0.0973	3.5770	7.8162
Tc-DHPE	*syn*	-1621.0934134	-0.0585	0.0717	3.5419	3.4610
	anti	-1621.0770927	-0.0515	0.0787	3.5430	9.9902
Tc-DHPB	*syn*	-1778.3302827	-0.0535	0.0778	3.5723	2.5907
	anti	-1778.3037676	-0.0503	0.0819	3.5960	10.4994
Tc-DHPP	*syn*	-1856.9565645	-0.0573	0.0742	3.5786	3.2090
	anti	-1856.9179688	-0.0570	0.0780	3.6733	7.3652

[a] E_T, E_{HOMO}, E_{LUMO}, and $\Delta E_{L\text{-}H}$ denote the total electronic energy, energies of the highest occupied molecular orbital (HOMO), the lowest unoccupied molecular orbital (LUMO) and the HOMO-LUMO gap, respectively.

Table 4. Atomic charge and spin density derived from MPA analysis for *syn*- and *anti*-Tc-DPs[a]

Complex	Tc-MDP	Tc-HMDP		Tc-HEDP		Tc-DHPE		Tc-DHPB		Tc-DHPP	
		syn	*anti*	*syn*	*anti*	*syn*	*anti*	*syn*	*anti*	*syn*	*anti*
Q_{Tc17}	1.292	1.363	1.342	1.326	1.318	1.333	1.325	1.349	1.330	1.333	1.227
Q_{O4}	-0.746	-0.731	-0.742	-0.735	-0.739	-0.762	-0.783	-0.816	-0.796	-0.795	-0.738
Q_{O6}	-0.758	-0.792	-0.778	-0.792	-0.764	-0.786	-0.740	-0.737	-0.749	-0.780	-0.733
Q_{O12}	-0.746	-0.726	-0.767	-0.745	-0.764	-0.788	-0.827	-0.792	-0.834	-0.805	-0.875
Q_{O14}	-0.758	-0.787	-0.751	-0.786	-0.756	-0.748	-0.773	-0.763	-0.773	-0.739	-0.827
Q_{O18}	-0.817	-0.772	-0.774	-0.775	-0.772	-0.827	-0.791	-0.822	-0.788	-0.823	-0.803
Q_{O19}	-0.817	-0.787	-0.767	-0.761	-0.788	-0.758	-0.793	-0.759	-0.790	-0.830	-0.688
ρ_{Tc17}	2.527	2.543	2.551	2.544	2.551	2.536	2.521	2.535	2.535	2.524	2.535
ρ_{O4}	0.106	0.074	0.074	0.049	0.084	0.093	0.038	0.107	0.039	0.083	0.080
ρ_{O6}	0.074	0.076	0.068	0.109	0.051	0.056	0.112	0.053	0.111	0.121	0.082
ρ_{O12}	0.106	0.060	0.070	0.050	0.070	0.114	0.004	0.097	0.022	0.086	0.011
ρ_{O14}	0.074	0.105	0.065	0.102	0.065	0.059	0.111	0.078	0.094	0.080	0.080
ρ_{O18}	0.017	0.029	0.055	0.032	0.051	0.013	0.072	0.015	0.040	0.005	0.005
ρ_{O19}	0.017	0.038	0.037	0.037	0.045	0.040	0.063	0.023	0.065	0.019	0.106

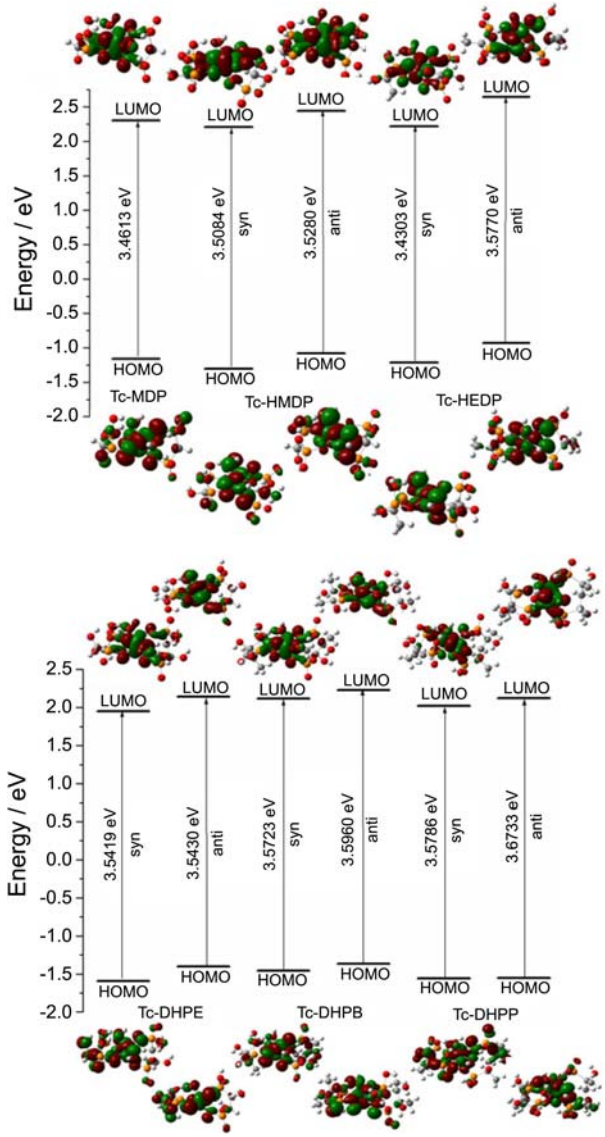

Figure 1. Frontier orbital diagrams of Tc-DPs calculated at the B3LYP/LANL2DZ level.

displays the energy level and contour plot of frontier molecular orbitals of Tc-DPs. Several similarities as well as important differences are evident along with the variation of substituents. Both the occupied and virtual orbitals in each complex are perturbed by different substituted groups, but the relative ordering and characters are not changed: HOMOs are contributed by predominant Tc $4d_{xy}$ and O 2p orbitals, while LUMOs are mainly composed of Tc $4d_{z2}$ orbitals mixed with little π*(P-O). As the tether between two phosphates increases to two or three, some 2p orbitals of C in the tether also have contributions to HOMOs besides $4d_{xy}$(Tc) and 2p(O), but the composition of LUMOs hardly changed. It seems that electron-donating substituent (–OH, $–CH_3$ and $–CH_2–$) has little effect on FMOs although there is relatively larger effect on HOMOs, because they are directly inserted into the ligand DP and far from the center metal Tc. However, noteworthy is that with the increase of electron-donating substituent or tether, the energy gap between FMOs increases on the whole. According to the above analysis of FMOs, it can be inferred that ranging from Tc-MDP to Tc-DHPP, the probability of non-radiative deactivation *via* d-d state decreases. In other words, introduction of σ-donor substituents to the MDP ligand will prohibit non-radiative pathways *via* d-d transitions in these complexes.

Focusing on the charge distribution of these Tc-DPs, one can find that the calculated charge on the technetium atom is considerable lower than the formal charge +4, corresponding d^3 configuration of the central ion. It results from significant charge donation from the ligands. The charges on the oxygen atoms which are coordinated to the technetium (*i.e.*, O4, O6, O12, O14, O18 and O19) are also significantly smaller than −2. On the whole, the charges on the oxygen atoms of the diphosphonate ligand are less negative in comparison with the oxygen atom of hydroxyl groups. It indicates the higher electron density delocalization from the O_{DP} towards the central ion and corresponds to differences in the bond lengths of Tc-O_{DP} and Tc-O_{OH}. Similarly, the oxygen atoms bonded to the phosphorus also carry non-negligible negative charges (*ca.* −0.7) and the phosphorus possesses a positive charge (*ca.* 1.3), which is also much smaller than the formal charge +5. In a word, this charge distribution can be attributed to the nephelauxetic effect, whereby ligand charge donation partially shields the metal d electrons from the central-ion nuclear charge and drives expansion of the d-electron "cloud".[35] It agrees well with the investigation of Pauling that "Stable M-L bond formation generally reduces the positive charge on the metal as well as the negative charge on the ligand."[36]

With an electron-donating substituent –OH introduced to the diphosphonate ligand, the net atomic charge on Tc increases significantly and those on O_{OH} decrease dramatically in comparison with the parent complex Tc-MDP. However, as more electron-donating substituents added to the ligand such as –OH, $–CH_3$ and $–(CH_2)_n–$, the charge on Tc decreases in comparison with Tc-HMDP and it changes slightly from Tc-HEDP to Tc-DHPP. This suggests that introduction of more electron-donating substituents has little effect on the charge distribution because they are far from the center metal Tc. A comparison of Q_{Tc} between *syn* and *anti* isomers shows that the former is relatively more positive than the latter, indicating the ligand-to-metal electron donation in the *anti* isomers is larger than that in the *syn* isomers.

In addition, MPA spin-unrestricted analysis also provides the atomic spin density ρ, which is the difference between the total α and β electronic populations of the atom. As for the complexes Tc-DPs, the spin densities are found to be mainly localized on the center metal Tc (*ca.* 2.5) and partly located on the six coordinated oxygen atoms (see Table 4). On those atoms that are not involved in direct bonding with the metal Tc, there is little spin density. This shows that the spin density is borne by the technetium atom and corresponds to the quartet d^3 state of the technetium atom in the title complex, implying that no metal-ligand back-donation exists at this level. Furthermore, it is also noted that introducing an electron-donating substituent (–OH, $–CH_3$) to the

Table 5. Biodistribution of ^{99m}Tc-DPs in rats (mean ± SD, n = 4, t = 0.5 h, %ID/g)

Complex	a_{bone}	a_{muscle}	a_{blood}	a_{bone}/a_{muscle}	a_{bone}/a_{blood}
Tc-MDP	22.42 ± 2.45	0.14 ± 0.01	0.59 ± 0.03	164.17	46.97
Tc-DHPE	18.23 ± 5.87	0.15 ± 0.05	0.55 ± 0.08	121.53	33.15
Tc-DHPB	6.03 ± 1.30	0.38 ± 0.05	2.18 ± 0.24	15.87	2.77
Tc-DHPP	5.67 ± 1.68	0.98 ± 0.15	1.01 ± 0.18	5.79	5.61

Table 6. Molecular geometrical parameters of Tc-DPs

Parameter	Tc-MDP	Tc-HMDP		Tc-HEDP		Tc-DHPE		Tc-DHPB		Tc-DHPP	
		syn	*anti*	*syn*	*anti*	*syn*	*anti*	*syn*	*anti*	*syn*	*anti*
V_{vdW}/cm^3·mol^{-1}	239.93	253.44	255.61	287.72	290.39	299.89	302.99	368.19	370.03	401.70	404.31
V_{sol}/cm^3·mol^{-1}	795.80	836.87	847.44	906.99	935.46	939.56	935.35	1091.60	1091.72	1177.29	1170.21
$SA_{grid,vdW}$/nm^2	339.24	353.84	363.71	393.92	408.37	404.78	411.01	480.87	482.51	523.46	525.89
$SA_{grid,sol}$/nm^2	484.75	502.19	510.68	521.13	542.60	546.66	536.52	596.41	592.77	634.65	623.38
$SA_{approx,vdW}$/nm^2	335.44	390.99	397.52	369.91	381.27	446.02	452.69	408.99	415.51	437.49	451.76
$SA_{approx,sol}$/nm^2	483.49	562.99	570.29	468.40	506.81	642.59	653.37	468.92	493.92	483.26	552.01
logP	6.74	6.74	6.74	7.60	7.60	5.59	5.59	8.07	8.07	7.10	7.10
$E_{hydration}$/kcal·mol^{-1}	-49.92	-58.59	-56.80	-52.24	-52.18	-55.45	-55.66	-45.20	-46.40	-39.68	-41.98

diphosphonate ligand leads to the increase of ρ_{Tc}. However, ρ_{Tc} decreases with more electron-donating substituents added to the diphosphonate ligand compared with Tc-HMDP and it changes little from Tc-DHPE to Tc-DHPP. This is consistent with the variation of Q_{Tc}.

Structure-Activity Relationship. Table 5 gives some important experimental biodistribution results of ^{99m}Tc-DHPE, ^{99m}Tc-DHPB and ^{99m}Tc-DHPP as well as ^{99m}Tc-MDP,[13] including the bone uptake (a_{bone}, %ID·g^{-1}), muscle uptake (a_{muscle}, %ID·g^{-1}), blood uptake (a_{blood}, %ID·g^{-1}), and uptake ratios of bone to soft tissues such as muscle (a_{bone}/a_{muscle}) and blood (a_{bone}/a_{blood}). Here, it should be pointed out that although there are many biodistribution studies reported for the approved radiopharmaceutical ^{99m}Tc-MDP in the past, the data for the organ uptake at the same time point are difficult to find. Therefore, to compare the biodistribution results more accurately, we carried out the biodistribution study for ^{99m}Tc-MDP using the same experimental method as ^{99m}Tc-DHPE.[11]

As can be seen from Table 5, the bone uptake of ^{99m}Tc-DHPE at 0.5 h post injection was markedly larger than those of ^{99m}Tc-DHPB and ^{99m}Tc-DHPP, and it decreases in the order of ^{99m}Tc-DHPE > ^{99m}Tc-DHPB > ^{99m}Tc-DHPP although the difference between latter two agents is small. At the same time, the muscle uptake and blood uptake of ^{99m}Tc-DHPE are both smaller than those of ^{99m}Tc-DHPB and ^{99m}Tc-DHPP. Therefore, the uptake ratios of bone to muscle and blood of ^{99m}Tc-DHPE are much higher than those of ^{99m}Tc-DHPB and ^{99m}Tc-DHPP. Analysis of their structures shows that the decrease in the bone uptake of ^{99m}Tc-DHPB and ^{99m}Tc-DHPP can be attributed to the steric hindrance of $-CH_3$. Compared with ^{99m}Tc-DHPB, additional methylene chain introduced to ^{99m}Tc-DHPP has little effect on the biological properties. For example, the additional methylene group did not change the bone uptake and uptake ratios of ^{99m}Tc-DHPP significantly. Therefore, it can be concluded that the side chain $-CH_3$ plays a dominant role in the organ uptake, which is not beneficial to improve the biological performance of ^{99m}Tc-DPs. Compared with the clinically widely-used bone imaging agent ^{99m}Tc-MDP, the radiotracer ^{99m}Tc-DHPE shows comparable characteristics including high selective uptake in the skeleton and low uptake in soft

Table 7. Linear regressions for activities and structures of *syn*-^{99m}Tc-labeled diphosphonate complexes

	a_{bone}	a_{muscle}	a_{bone}/a_{muscle}
*E*g	515.75-142.05*E*g R = -0.898, SD = 4.603	-16.55+4.79*E*g R = 0.656, SD = 0.365	4742.41-1318.51*E*g R = -0.908, SD = 40.166
V_{vdW}	50.82-0.12 V_{vdW} R = -0.974, SD = 2.378	-1.10+0.005V_{vdW} R = 0.843, SD = 0.260	426.15-1.07 V_{vdW} R = -0.982, SD = 17.935
V_{sol}	62.20-0.05 V_{sol} R = -0.969, SD = 2.590	-1.576+0.002V_{sol} R = 0.849, SD = 0.255	531.89-0.45V_{sol} R = -0.978, SD = 19.879
$SA_{grid,vdW}$	57.44-0.10 $SA_{grid,vdW}$ R = -0.971, SD = 2.498	-1.396+0.004$SA_{grid,vdW}$ R = 0.857, SD = 0.249	487.70-0.94$SA_{grid,vdW}$ R = -0.980, SD = 19.002
$SA_{grid,sol}$	84.01-0.13 $SA_{grid,sol}$ R = -0.953, SD = 3.166	-2.51+0.01$SA_{grid,sol}$ R = 0.850, SD = 0.254	735.69-1.16$SA_{grid,sol}$ R = -0.965, SD = 25.260

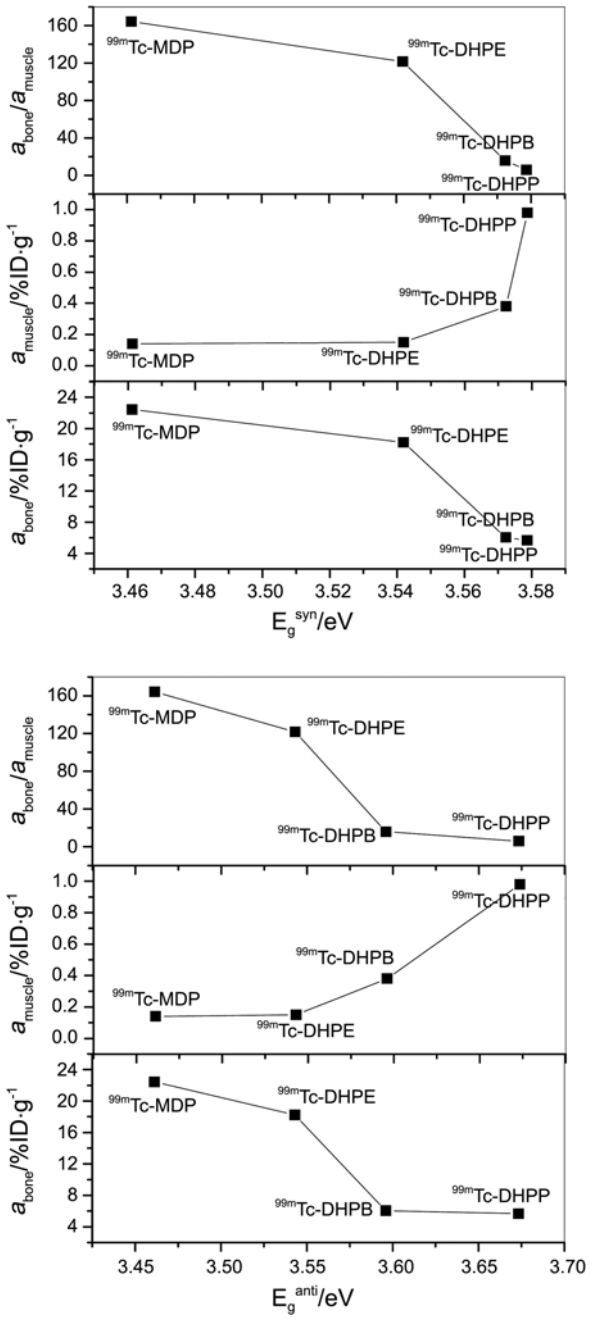

Figure 2. Correlations between biological properties and the FMO energy gap E_g.

tissues, suggesting that it holds great potential as a novel tracer for bone scanning.

Based on the calculated geometric and electronic parameters, the structure-activity relationship (SAR) was investigated for ^{99m}Tc-DPs. The geometric descriptor includes two types of molecular volume V_{vdW} and V_{sol} (van der Waals and solvent-accessible bounding surface), four types of molecular surface area $SA_{grid,vdW}$ (van der Waals surface area using a grid method), $SA_{grid,sol}$ (solvent-accessible area using a grid method), $SA_{approx,vdW}$ (van der Waals surface area using a fast approximate method) and $SA_{approx,sol}$ (solvent-accessible area using a fast approximate method), which have been listed in Table 6. The electronic descriptor includes E_{HOMO}, E_{LUMO}, E_g, μ, Q_{Tc}, ρ_{Tc}, logP and $E_{hydration}$. The biological descriptor consists of the bone uptake, muscle uptake, and bone/muscle uptake ratio, since they are more important for obtaining good quality skeletal image than the blood uptake and bone/blood ratio.

As shown in Figures 2 and 3, the biological performance correlates well with the FMO energy gap E_g and molecular geometrical parameters V_{vdW}, V_{sol}, $SA_{grid,vdW}$ and $SA_{grid,sol}$. These correlations can be expressed in the linear form of Y = a+bX, which have been summarized in Tables 7 and 8. It is clear that with the increase of E_g, V_{vdW}, V_{sol}, $SA_{grid,vdW}$ and $SA_{grid,sol}$, the bone uptake and bone/muscle ratio both decrease in the order of ^{99m}Tc-MDP > ^{99m}Tc-DHPE > ^{99m}Tc-DHPB > ^{99m}Tc-DHPP, while the muscle uptake increases in the order of ^{99m}Tc-MDP < ^{99m}Tc-DHPE < ^{99m}Tc-DHPB < ^{99m}Tc-DHPP. These can be explained by the following two facts. On the one hand, diphosphonates are very stable synthetic analogues of pyrophosphates and exhibit high affinities for calcified matrices in bone, such as hydroxyapatite (HA).[37] So, when the radiotracers ^{99m}Tc-DPs arrive at the bone surface, they will interact with HA and new chemical bonds will form between the multi-dental diphosphonate complexes and the calcium ion Ca^{2+} of HA. Hence, it leads to the bone uptake of ^{99m}Tc-DPs. As well known, if the FMO energy gap of the compound is larger, its stability is higher and its reaction activity is lower.[38] So, ^{99m}Tc-labeled diphosphonate complex with a larger E_g value is more difficult to interact with HA and the bone uptake is therefore smaller. On the other hand, if the molecular volume and surface area of the bone-targeting compound is smaller, there will be more adsorption sites on the HA. As a result, the bone uptake increases.

In summary, it is beneficial to improve the bone imaging efficiency by decreasing the FMO energy gap, molecular volume or surface area of ^{99m}Tc-labeled diphosphonate complex. Furthermore, according to the established SAR and calculated results, it can be inferred that the bone uptakes and bone/muscle ratios of ^{99m}Tc-HMDP and ^{99m}Tc-HEDP may be lower than that of ^{99m}Tc-MDP and higher than those of ^{99m}Tc-DHPE, ^{99m}Tc-DHPB and ^{99m}Tc-DHPP, *i.e.*, ^{99m}Tc-MDP > ^{99m}Tc-HMDP > ^{99m}Tc-HEDP > ^{99m}Tc-DHPE > ^{99m}Tc-DHPB > ^{99m}Tc-DHPP.

Conclusions

In this study, theoretical calculations were performed to investigate the substituent effect on the geometric and electronic structures as well as the biological properties of ^{99m}Tc-labled diphosphonate complexes. With the electron-donating substituent or tether between phosphate groups increasing, the frontier orbital energy gap increases and the reaction activity decreases. The biological properties correlate well with the FMO energy gap, molecular volume and surface area of the complex. With the decrease of the FMO energy gap, molecular volume and surface area of ^{99m}Tc-DPs, the bone uptake and bone/muscle uptake ratio increase while the

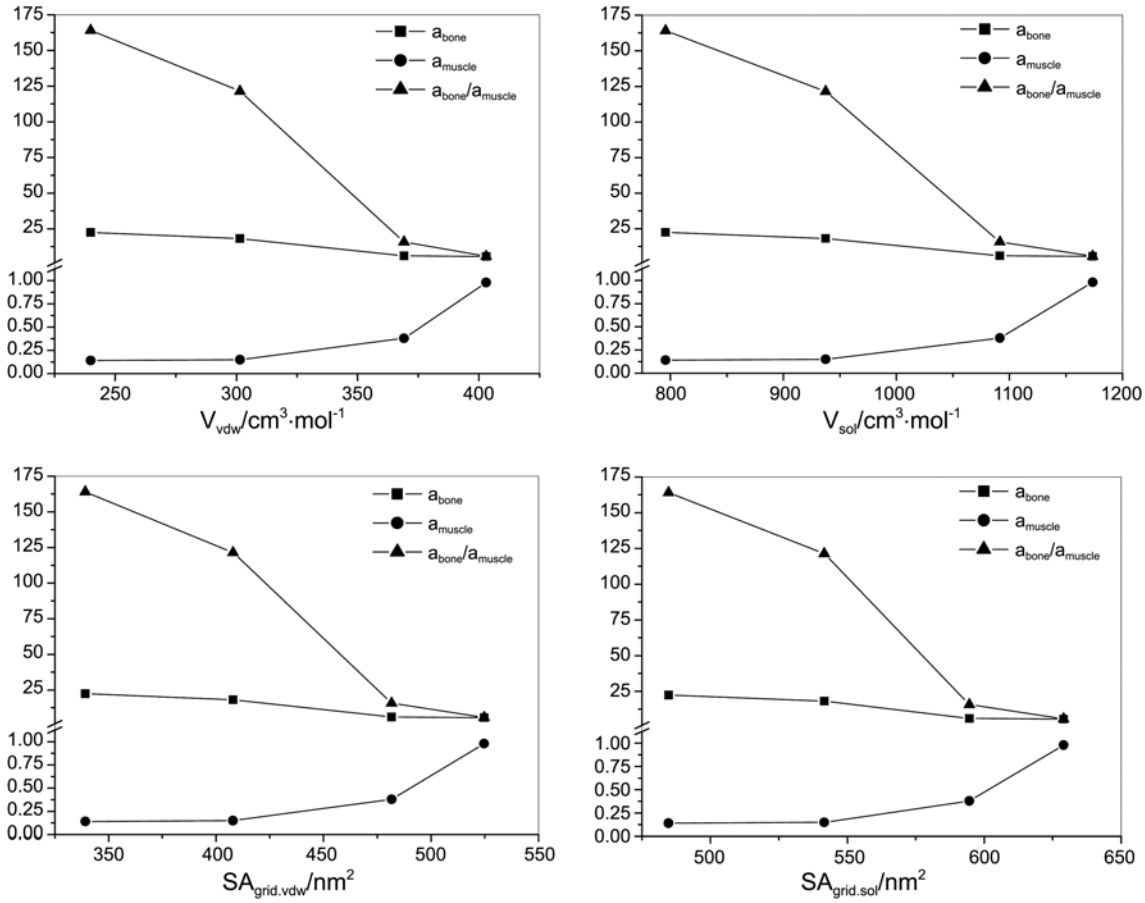

Figure 3. Correlations between biological properties and molecular geometrical parameters.

Table 8. Linear regressions for activities and structures of *anti*-^{99m}Tc-labeled diphosphonate complexes

	a_{bone}	a_{muscle}	a_{bone}/a_{muscle}
Eg	327.32-88.06*Eg* R = -0.921, SD = 4.073	-13.71+3.96*Eg* R = 0.895, SD = 0.215	3009.11-821.73*Eg* R = -0.936, SD = 33.641
V_{vdW}	50.49-0.11V_{vdW} R = -0.971, SD = 2.494	-1.08+0.005V_{vdW} R = 0.840, SD = 0.262	423.25-1.05 V_{vdW} R = -0.980, SD = 19.030
V_{sol}	62.83-0.05V_{sol} R = -0.973, SD = 2.418	-1.58+0.002V_{sol} R = 0.844, SD = 0.259	537.40-0.46 V_{sol} R = -0.982, SD = 18.297
$SA_{grid,vdW}$	57.25-0.10$SA_{grid,vdW}$ R = -0.965, SD = 2.723	-1.38+0.004 $SA_{grid,vdW}$ R = 0.850, SD = 0.254	486.27-0.93 $SA_{grid,vdW}$ R = -0.975, SD = 21.119
$SA_{grid,sol}$	88.53-0.13$SA_{grid,sol}$ R = -0.970, SD = 2.527	-2.63+0.005 $SA_{grid,sol}$ R = 0.848, SD = 0.256	775.70-1.25 $SA_{grid,sol}$ R = -0.980, SD = 19.302

muscle uptake decreases. This may be instructive for the design and synthesis of novel ^{99m}Tc-diphosphonate bone imaging agents.

Acknowledgments. We are very grateful for the financial support from the National Natural Science Foundation of China (20801024, 21001055), Natural Science Foundation of Jiangsu Province (BK2009077), and Key Medical Talent Project of Jiangsu Province (RC2011097).

Supplementary Data. Plots of optimized ground-state geometries of ^{99m}Tc-MDP, ^{99m}Tc-HMDP, ^{99m}Tc-HEDP, ^{99m}Tc-DHPE, ^{99m}Tc-DHPB and ^{99m}Tc-DHPP at the B3LYP/LANL2DZ level (Figure 1S).

References

1. Dilworth, J. R.; Parrott, S. J. *Chem. Soc. Rev.* **1998**, *27*, 43.
2. Kodina, G. E. In *Isotopes. Properties, Obtaining, Applications*; Baranov, V. Y., Ed.; Atomnaya Energiya: Moscow, 2000.
3. Méndez-Rojas, M. A.; Kharisov, B. I.; Tsivadze, A. Y. *J. Coord. Chem.* **2006**, *59*, 1.
4. Jurisson, S. S.; Lydon, J. D. *Chem. Rev.* **1999**, *99*, 2205.
5. Pauwels, E. K.; Stokkel, M. P. *Q. J. Nucl. Med.* **2001**, *45*, 18.
6. Bartholom, M. D.; Louie, A. S.; Valliant, J. F.; Zubieta, J. *Chem.*

Rev. **2010**, *110*, 2903.
7. Subramanian, G.; McAfee, J. G.; Blair, R. J.; Kallfelz, F. A.; Thomas, F. D. *J. Nucl. Med.* **1975**, *16*, 744.
8. Bevan, J. A.; Tofe, A. J.; Benedict, J. J.; Francis, M. D.; Barnett, B. L. *J. Nucl. Med.* **1980**, *21*, 961.
9. Love, C.; Din, A. S.; Tomas, M. B.; Kalapparambath, T. P.; Palestro, C. J. *Radiographics.* **2003**, *23*, 341.
10. (a) Láznícek, M.; Láznícková, A.; Budský, F. *Nucl. Med. Commun.* **1996**, *17*, 1016. (b) Fueger, B. J.; Mitterhauser, M.; Wadsak, W.; Ofluoglu, S.; Traub, T.; Karanikas, G.; Dudczak, R.; Pirich, C. *Nucl. Med. Commun.* **2004**, *25*, 361. (c) El-Mabhouh, A. A.; Angelov, C. A.; Cavell, R.; Mercer, J. R. *Nucl. Med. Biol.* **2006**, *33*, 715. (d) Palma, E.; Oliveira, B. L.; Correia, J. D.; Gano, L.; Maria, L.; Santos, I. C.; Santos, I. *J. Biol. Inorg. Chem.* **2007**, *12*, 667. (e) Asikoglu, M.; Durak, F. G. *Appl. Radiat. Isotopes.* **2009**, *67*, 1616.
11. (a) Guo, X. H.; Luo, S. N.; Wang, H. Y.; Zhou, L.; Xie, M. H.; Ye, W. Z.; Yang, M.; Wang, Y. *Nucl. Sci. Tech.* **2006**, *17*, 285. (b) Chen, C. Q.; Luo, S. N.; Lin, J. G.; Yang, M.; Ye, W. Z.; Qiu, L.; Sang, G. M.; Xia, Y. M. *Nucl. Sci. Tech*. **2009**, *20*, 302. (c) Lin, J. G.; Luo, S. N.; Chen, C. Q.; Qiu, L.; Wang, Y.; Cheng, W.; Ye, W. Z.; Xia, Y. M. *Appl. Radiat. Isotopes.* **2010**, *68*, 1616. (d) Wang, Y.; Luo, S. N.; Lin, J. G.; Qiu, L.; Cheng, W.; Zhai, H. Z.; Nan, B. B.; Ye, W. Z.; Xia, Y. Y. *Appl. Radiat. Isotopes.* **2011**, *69*, 1169. (e) Lin, J. G.; Qiu, L.; Cheng, W.; Luo, S. N.; Ye, W. Z. *Nucl. Med. Biol.* **2011**, *38*, 619. (f) Qiu, L.; Cheng, W.; Lin, J. G.; Luo, S. N.; Xue, L. *Molecules* **2011**, *16*, 6165. (g) Lin, J. G.; Qiu, L.; Cheng, W.; Luo, S. N.; Xue, L.; Zhang, S. *Appl. Radiat. Isotopes.* **2012**, *70*, 848.
12. Archimandritis, S. C.; Tsolis, A. K. *Eur. J. Nucl. Med.* **1987**, *13*, 134.
13. Lu, G. X.; Chen, H. Y. *Nucl. Tech.* **1999**, *22*, 682.
14. Chen, K. X.; Jiang, H. L.; Ji, R. Y. *Computer Aided Drug Design: Principles, Methods and Applications*; Shanghai Scientific and Technology Press: Shanghai, 2000.
15. (a) Qiu, L.; Lin, J. G.; Ju, X. H.; Gong, X. D.; Luo, S. N. *Chinese J. Chem. Phys.* **2011**, *24*, 295. (b) Qiu, L.; Lin, J. G.; Gong, X. D.; Ju, X. H.; Luo, S. N. *B. Korean Chem. Soc.* **2011**, *32*, 2358.
16. (a) Fan, H. J.; Hall, M. B. *Organometallics* **2001**, *20*, 5724. (b) Safi, B.; Mertens, J.; Proft, F. D.; Alberto, R.; Geerlings, P. *J. Phys. Chem. A* **2005**, *109*, 1944. (c) Safi, B.; Mertens, J.; Proft, F. D.; Alberto, R.; Geerlings, P. *J. Phys. Chem. A* **2006**, *110*, 9240. (d) Cundari, T. R.; Grimes, T. V.; Gunnoe, T. B. *J. Am. Chem. Soc.* **2007**, *129*, 13172. (e) Riedel, S.; Renz, M.; Kaupp, M. *Inorg. Chem.* **2007**, *46*, 5734. (f) Haunschild, R.; Frenking, G. *J. Organomet. Chem.* **2008**, *693*, 3627. (g) Safi, B.; Mertens, J.; Kersemans, K.; Geerlings, P. *Nucl. Med. Biol.* **2008**, *35*, 747. (h) Jia, H. M.; Fang, D. C.; Feng, Y.; Zhang, J. Y.; Fan, W. B.; Zhu, L. *Theor. Chem. Account.* **2008**, *121*, 271. (i) Ess, D. H. *J. Org. Chem.* **2009**, *74*, 1498. (j) Saeki, M.; Sasaki, Y.; Nakai, A.; Ohashi, A.; Banerjee, D.; Scheinost, A.; Foerstendorf, H. *Inorg. Chem.* **2012**, *51*, 5814.
17. Jurisson, S.; Berning, D.; Jia, W.; Ma, D. S. *Chem. Rev.* **1993**, *93*, 1137.
18. Subramanian, G.; McAfee, J. G.; Blair, R. J.; Mehter, A.; Connor, T. *J. Nucl. Med.* **1972**, *13*, 947.
19. Libson, K.; Deutsch, E.; Barnett, B. L. *J. Am. Chem. Soc.* **1980**, *102*, 2476.
20. Materials Studio 3.0.1; Accelrys Inc.: San Diego, CA, 2004.
21. Rappé, A. K.; Casewit, C. J.; Colwell, K. S.; Goddard, W. A.; Skiff, W. M. *J. Am. Chem. Soc.* **1992**, *114*, 10024.
22. (a) Becke, A. D. *J. Chem. Phys.* **1993**, *98*, 5648. (b) Lee, C.; Yang, W.; Parr, R. G. *Phys. Rev. B* **1988**, *37*, 785.
23. Frisch, M. J.; Trucks, G. W.; Schlegel, H. B.; Scuseria, G. E.; Robb, M. A.; Cheeseman, J. R.; Montgomery, J. A., Jr.; Vreven, T.; Kudin, K. N.; Burant, J. C.; Millam, J. M.; Iyengar, S. S.; Tomasi, J.; Barone, V.; Mennucci, B.; Cossi, M.; Scalmani, G.; Rega, N.; Petersson, G. A.; Nakatsuji, H.; Hada, M.; Ehara, M.; Toyota, K.; Fukuda, R.; Hasegawa, J.; Ishida, M.; Nakajima, T.; Honda, Y.; Kitao, O.; Nakai, H.; Klene, M.; Li, X.; Knox, J. E.; Hratchian, H. P.; Cross, J. B.; Adamo, C.; Jaramillo, J.; Gomperts, R.; Stratmann, R. E.; Yazyev, O.; Austin, A. J.; Cammi, R.; Pomelli, C.; Ochterski, J. W.; Ayala, P. Y.; Morokuma, K.; Voth, G. A.; Salvador, P.; Dannenberg, J. J.; Zakrzewski, V. G.; Dapprich, S.; Daniels, A. D.; Strain, M. C.; Farkas, O.; Malick, D. K.; Rabuck, A. D.; Raghavachari, K.; Foresman, J. B.; Ortiz, J. V.; Cui, Q.; Baboul, A. G.; Clifford, S.; Cioslowski, J.; Stefanov, B. B.; Liu, G.; Liashenko, A.; Piskorz, P.; Komaromi, I.; Martin, R. L.; Fox, D. J.; Keith, T.; Al-Laham, M. A.; Peng, C. Y.; Nanayakkara, A.; Challacombe, M.; Gill, P. M. W.; Johnson, B.; Chen, W.; Wong, M. W.; Gonzalez, C.; Pople, J. A. Gaussian 03, Revision C.02; Gaussian, Inc.: Wallingford, CT, 2004.
24. Hay, P. J.; Wadt, W. R. *J. Chem. Phys.* **1985**, *82*, 299.
25. Dunning, T. H., Jr.; Hay, P. J. *Modern Theoretical Chemistry*, Schaefer, H. F., III, Ed.; Plenum: New York, 1976; Vol. 3, p 1.
26. Hay, P. J.; Wadt, W. R. *J. Chem. Phys.* **1985**, *82*, 270.
27. Mulliken, R. S. *J. Chem. Phys.* **1955**, *23*, 1833.
28. GaussView, release 3.0; Gaussian Inc.: Pittsburgh, PA, 2003.
29. HyperChem, release 7.5; Hypercube Inc.: NewYork, 2003.
30. Thomas. R. W.; Estes, G. W.; Elder, R. C.; Deutsch, E. *J. Am. Chem. Soc.* **1979**, *101*, 4581.
31. Turki, M.; Daniel, C.; Stufkens, D. J. *J. Am. Chem. Soc.* **2001**, *123*, 11431.
32. DeLaMatter, D.; McCullough, J. J.; Calvo, C. *J. Phys. Chem.* **1973**, *77*, 1146.
33. (a) Uchtman, V. A.; Gloss, R. A. *J. Phys. Chem.* **1972**, *76*, 1298. (b) Uchtman, V. A. *J. Phys. Chem*. **1972**, *76*, 1304. (c) Räsänen, J. P.; Pohjala, E.; Nikander, H.; Pakkanen, T. A. *J. Phys. Chem. A* **1997**, *101*, 5196.
34. Alberto, R.; Schibli, R.;,Waibel, R.; Abram,U.; Schubiger, P. A. *Coord. Chem. Rev.* **1999**, *190-192*, 901.
35. Schäffer, C. E. *Inorg. Chim. Acta* **2000**, *300-302*, 1035.
36. Pauling, L. C. In *The Nature of the Chemical Bond*, 3rd ed.; Cornell University Press: Ithaca, NY, 1960; p 172.
37. Fleisch, H.; Russell, R. G. G.; Straumann, F. *Nature* **1966**, *26*, 901.
38. Fukui, K. *Theory of Orientation and Stereoselection, Reactivity and Structure, Concepts in Organic Chemistry*; Springer: Berlin, 1975, Vol. 2.